Performance analysis of a swept-source optical coherence tomography system with a quadrature interferometer and optical amplification

Mao, Youxin; Flueraru, Costel; Chang, Shoude; Popescu, Dan P.; Sowa, Michael G.

Publisher's version / la version de l'éditeur:
Optics Communications, 284, pp. 2622-2627, 2011-01-11

Web page / page Web
http://dx.doi.org/10.1016/j.optcom.2011.01.016
http://nparc.cisti-icist.nrc-cnrc.gc.ca/npsi/ctrl?action=rtdoc&an=17400968&lang=en
http://nparc.cisti-icist.nrc-cnrc.gc.ca/npsi/ctrl?action=rtdoc&an=17400968&lang=fr

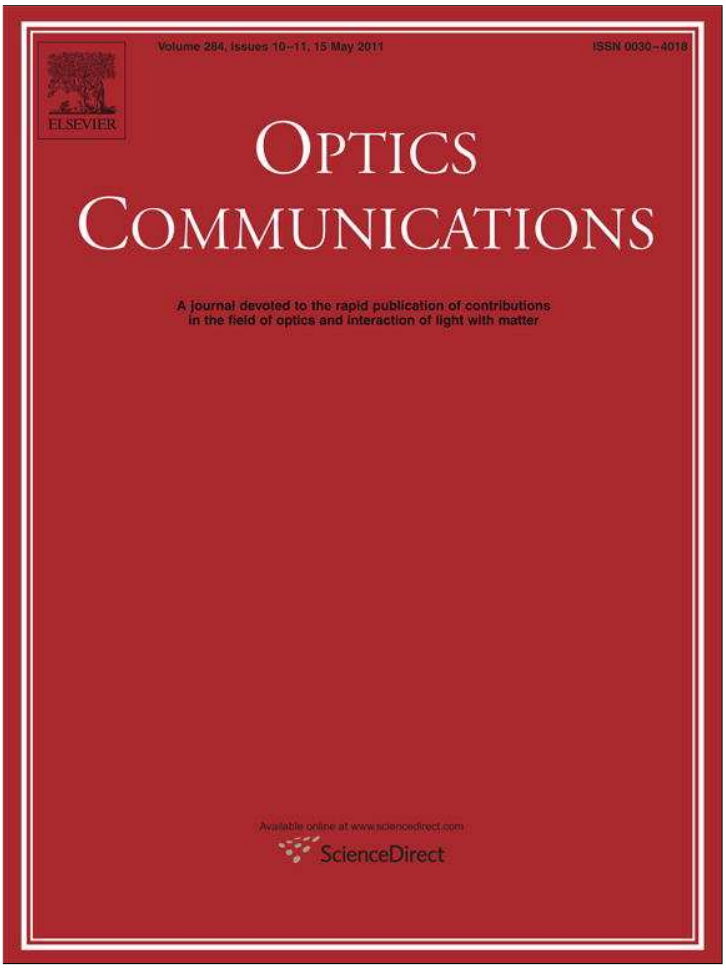

Optics Communications 284 (2011) 2622–2627

Contents lists available at ScienceDirect

Optics Communications

journal homepage: www.elsevier.com/locate/optcom

Performance analysis of a swept-source optical coherence tomography system with a quadrature interferometer and optical amplification

Youxin Mao [a,*], Costel Flueraru [a], Shoude Chang [a], Dan P. Popescu [b], Michael G. Sowa [b]

[a] Institute for Microstructural Sciences, National Research Council Canada, 1200 Montreal Rd, Ottawa, ON, Canada K1A 0R6
[b] Institute for Biodiagnostics, National Research Council Canada, 435 Ellice Avenue, Winnipeg, MB, Canada R3B 1Y6

ARTICLE INFO

Article history:
Received 12 October 2010
Received in revised form 6 January 2011
Accepted 11 January 2011
Available online 25 January 2011

Keywords:
Optical coherence tomography
Quadrature interferometer
Semiconductor optical amplifier
Medical
Biological imaging

ABSTRACT

A performance analysis of signal to noise ratio for an optical coherence tomography system with quadrature detection and a semiconductor optical amplifier in the sample arm is discussed. The results are compared and discussed in relation to a conventional OCT system (without optical amplification). An increase of the signal to noise ratio up to 14 dB at a depth of 0.5 mm is obtained compared to the system without the optical amplifier. Overall, an improvement was demonstrated for signal coming from deeper regions within the samples. Arterial plaque from a myocardial infarction-prone Watanabe heritable hyperlipidemic (WHHLMI) rabbit is visualized and characterized using this system. Improvement of signal to noise ratio increases the penetration depth possible for OCT images, from 1 mm to 2 mm within the vessel wall of an artery. Preliminary results show that vulnerable plaque with fibrous cap, macrophage accumulations and calcification in the arterial tissue are measurable with this OCT system.

1. Introduction

Optical coherence tomography (OCT) [1] is an emerging non-invasive cross-sectional imaging modality for visualizing subsurface tissue details in vivo at resolutions approaching histology [2]. OCT is analogous to ultrasound, measuring the backreflection of infrared light rather than sound. The advantages of OCT compared to ultrasound include its higher resolution, video speed acquisition rate, compactness and portability. When a small and inexpensive optical fiber probe as an optical catheter constitutes the sample arm, the system becomes suitable for intra-vascular probing. Because OCT uses light, a variety of functional and spectroscopic techniques are available to expand its capabilities, including polarization, absorption, elastography, Doppler, and dispersion analysis. An OCT system with higher signal-to-noise ratio (SNR) is essentially important for imaging turbid environments, such as biological tissues, because the back-scattered signals from these types of samples are extremely weak. Swept-source OCT (SS-OCT) has received much attention in recent years not only because of its higher SNR at high imaging speeds but also for its imaging possibilities in the 1300 nm wavelength range, where the reduced light scattering by tissue enables OCT to collect signal from deeper into tissue compared to OCT imaging based on shorter source wavelengths. Several interferometric platforms have been proposed by using multi-port fiber couplers such as the 3×3 quadrature interferometer [3]. Measuring instantaneous complex signals by using a 3×3 quadrature interferometer one can suppress the complex conjugate artifact and therefore double the effective imaging depth [4]. The phase information of the complex interferometric signals can also be exploited to gain additional information about the tissue, to enhance image contrast and to perform quantitative measurements. In addition, the Mach–Zehnder configuration of the presented interferometric setup (MZI) allows different options to distribute optical power between the reference and sample arms. An unbalanced input directs more optical power from the light source to the sample than that to the reference mirror [5] while the balanced detection is used to reduce the excess intensity noise [6]. Both techniques play their parts in increasing SNR. However in the case of imaging biomedical samples, the signal backscattered from tissue is much weaker than the reference signal so an attenuation of optical power in the reference arm is required in order to increase the SNR. On the other hand, only by increasing the power of the light source does not efficiently result into an SNR increase [7].

The ability of OCT to image vascular plaque has been previously demonstrated [8–12]. However, OCT images of the arterial wall are limited to depths of ~1 mm even using the Fourier domain methods [2]. The limited imaging depth into the vascular wall is one of the most serious limitations for OCT to be used as a routine clinical intravascular imaging method. Further improvement of the SNR of OCT is needed in order to increase the imaging depth of OCT into tissue. Adding an optical amplifier in the path of the backscattered signal in the sample arm of a SS-OCT system with a balanced Michelson interferometer has been proposed [13]. Experimental results have been reported from SS-OCT systems using a 2×2 MZI

* Corresponding author.
E-mail address: Linda.Mao@nrc-cnrc.gc.ca (Y. Mao).

0030-4018/$ – see front matter.
doi:10.1016/j.optcom.2011.01.016

[14,15]. In these configurations the noise level is also amplified together with the signal leading about 2 dB SNR improvement.

In this paper, a SS-OCT system with a quadrature interferometer (QSS-OCT) using a semiconductor optical amplifier (SOA) for the amplification of the weak signal existent in the sample arm is demonstrated both theoretically and experimentally. Comparing the OCT system operation with and without the amplifier, shows an increase in SNR up to 14.1 dB and 18.3 dB at 0.5 mm and 4 mm depths, respectively. Lipid-rich plaque of a WHHLMI rabbit is visualized and characterized with this system. Preliminary results show that vulnerable plaque with fibrous cap, macrophage accumulations and calcification in the arterial tissue are measurable with our OCT system, which is also able to image features located as deep as two millimetres from the lumen surface.

2. Swept source OCT with quadrature interferometer and optical amplification

Fig. 1(a) shows an experimental setup of our QSS-OCT system that uses a balanced 3×3 and 2×2 quadrature MZI and an SOA for weak sample signal amplification. The swept laser source (HSL2000-HL, Santac) used in the setup had a central wavelength of 1320 nm and a full scan wavelength range of 110 nm, was swept linearly in optical frequency with a linearity of 0.2%. The bandwidth of the source corresponds to an 8-μm OCT imaging resolution in the air. The average output power and coherence length of the swept source were 12 mW and 10 mm, respectively. A repetition scan rate of 20 kHz was used in our system and the related duty cycle was 68%. The light output from the swept laser source was launched first into the 2×2 coupler where 90% of the power was diverted toward the sample. The reference arm was arranged with a fiber collimator and a mirror. The light was directed to the sample through a lensed single mode fiber probe [16]. Since SOA amplifies both coherent and incoherent back-reflected lights the first surface reflection from the optical probe is important. In this report we used a home-build ball lens probe with extremely low reflectivity (~−55 dB). A galvanometer (Blue Hill Optical technologies) scanned the fiber probe along the sample surface up to 4 mm-long trip corresponding to an OCT image width of 900 pixels. The weak light back-scattered from the sample was fed into an SOA (Covega) whose gain can be adjusted by a variable attenuator connected after the SOA. The SOA had the same center wavelength and bandwidth as the swept source. The gain could be varied up to 35 dB. Normalized spectra of light source reflected from reference arm (solid line) and amplified sample arm (dot line) were measured as shown in Fig. 1(b). 3 dB bandwidths of 98.6 nm and 98.4 nm were measured in reference and sample arms, respectively. This small change of the measured bandwidths indicates the wavelength dependent gain of the SOA has a small influence on the OCT image quality. The reference arm has been built so that it can match the optical distance of the sample arm without SOA and by adding an optical jumper with certain length it can match the optical distance of the sample arm with SOA. Both, the SOA and the added optical jumper (part of reference arm) could be removed allowing the system to be switched back to a regular QSS-OCT system without sample signal amplification [4,17]. A polarization controller was inserted before the SOA for optimal amplification. The amplified signal was combined with the signal returning from the reference mirror through the 3×3 and 2×2 couplers, thus implementing a dual-channel balanced detection system with two complementary components of the complex interferometric signals which suppresses the complex

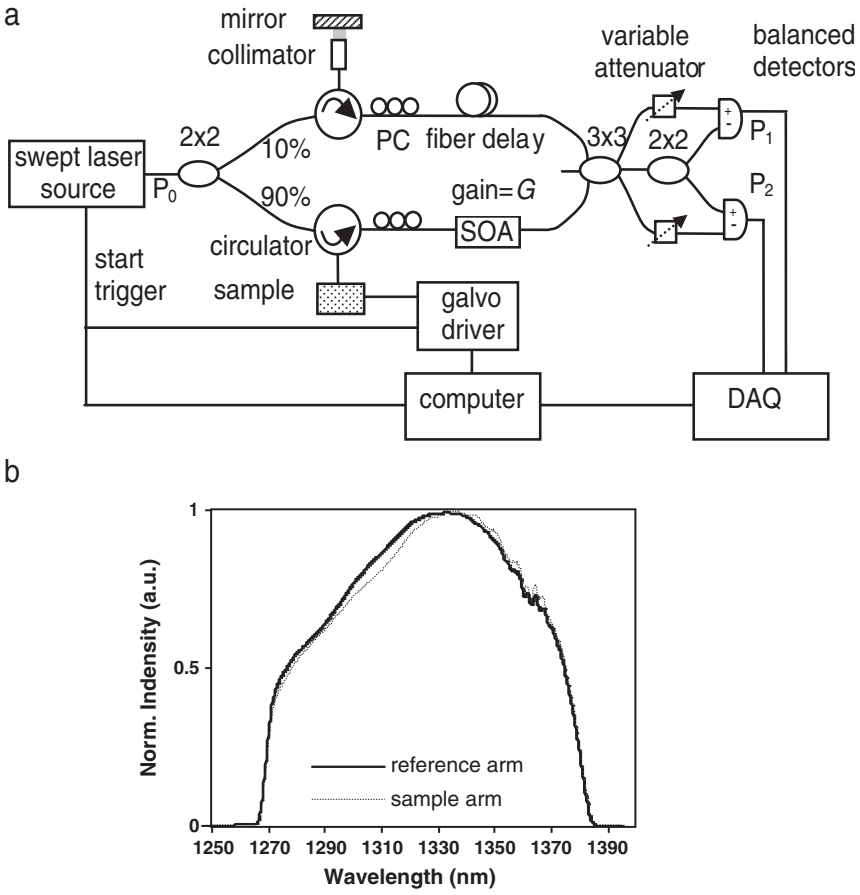

Fig. 1. (a) Experimental setup of our QSS-OCT system with a balanced 3×3 and 2×2 quadrature MZI and an SOA for the amplification of the signal back-scattered from the sample. (b) Measured normalized spectra of light source reflected from reference arm (solid line) and amplified sample arm (dot line).

conjugate artefact. Two attenuators were used to match the optical power entering the balanced detectors. Both balanced detectors (PDB150C, Thorlabs) used in this system had saturation powers of 5 mW. We selected a 3 dB bandwidth of 50 MHz to give sufficient imaging depth. The two detector outputs were digitized using a data acquisition card (DAQ) (PCI 5122, National Instruments) with 14-bit resolution and acquired signal at a sampling speed of 100 MS/s. The swept source generated a start trigger signal that was used to initiate the function generator for the galvo scanner and initiate the data acquisition process for each A-scan. Because the swept source was linearly swept with the wave-number k, A-scans data with resolved complex conjugate artifact were obtained by a direct inverse Fourier transformation (IFT) from the DAQ sampled data without performing an additional re-sampling step.

A phase difference ($\Delta\phi$) of 61° between the two output signals P_1 and P_2 was obtained. The real (P_{RE}) and imaginary (P_{IM}) part of the signals, e.g. quadrature components at phases 0° and 90°, were formed from the measured P_1 and P_2 using the following trigonometric equations [3,4]:

$$P_{RE} = P_1 \tag{1}$$

$$P_{IM} = \frac{P_1\ cos(\Delta\phi) - P_2}{sin(\Delta\phi)}. \tag{2}$$

The complex conjugate artifacts were suppressed by taking the complex inverse Fourier transformation of the quadrature components of the signals.

3. Signal to noise ratio analysis

Signal-to-noise (SNR) analysis of the interferometric platform has followed the OCT development. The pioneering work in setting the stage for comparison between time domain OCT setups was reported by Rollins and Izatt [5] and Podoleanu [6]. As the interest in Fourier domain and swept source OCT has grown several groups independently proposed method to compare and translate the signal-to-noise results between time domain and Fourier domain systems [18–20]. In this report we present an SNR analysis of our quadrature interferometric platform as integrated into a time domain system [5] followed by the correction proposed by Choma et al. [20] to translate the SNR results for a SS-OCT.

Assuming that the signal in the sample arm is coming from a single reflector located at the depth of z_0, then the two channel currents on the positive and negative photodiodes in each balanced detector when the SOA is inserted into the sample arm are given by:

$$I_{1\pm}(k_m, G) = \alpha\Big[P_{r\pm}(k_m) + P_{s\pm}(k_m, G) + P_{SP\pm}(G) \pm 2\sqrt{P_{r\pm}(k_m)P_{s\pm}(k_m, G)}\ cos\left(2k_m z_0 + \phi_\pm\right)\Big] \tag{3}$$

$$I_{2\pm}(k_m, G) = \alpha\Big[P_{r\pm}(k_m) + P_{s\pm}(k_m, G) + P_{SP\pm}(G) \pm 2\sqrt{P_{r\pm}(k_m)P_{s\pm}(k_m, G)}\ cos\left(2k_m z_0 + \phi_\pm + \Delta\phi\right)\Big] \tag{4}$$

where, $\alpha = \eta e/(h\nu_0)$ is photodiode photon-electron conversion factor, η is the quantum efficiency of the detector, e is the electronic charge, h is the Planck's constant, ν_0 is the mean frequency of the incident light, $P_r(k_m)$ is the optical signal power from the reference arm arriving at the photodiodes when wavenumber $k = k_m$, $P_s(k_m,G)$ is the amplified optical signal power from the sample arm at the photodiodes when wavenumber $k = k_m$, $P_{sp}(G)$ is the spontaneous emission power of the SOA recorded at the photodiodes, G is the gain of SOA, ϕ is an arbitrary phase shift, $\Delta\phi$ is the phase shift between the two output signals, $m = 1, 2, \ldots, M$, where M is the total sampling number of the axial pixels. Balanced detection subtracts each positive and negative current for each channel shown in Eqs. (3) and (4), so that the common DC parts are subtracted and the opposite AC parts are added. The complementary phase components of the signals can be calculated by Eqs. (1) and (2) for a complex discrete Fourier transform (DFT). Then, the maximum-squared signal power in our system with the dual-balanced quadrature detection is given as [5,21]:

$$\langle I(G)^2\rangle \approx (4D\alpha)^2 \cdot k_1 \cdot (1-k_1) \cdot k_2^2 \cdot S \cdot (1-X)^2 \cdot R \cdot G \cdot P_0^2 \tag{5}$$

where the brackets denote the ensemble average, k_1 and k_2 are the splitting ratios of the first and second optical coupler, R is the optical power reflectance of the reference mirror, X and S are the incoherent and coherence optical reflectance of the sample, G is the optical gain of SOA, P_0 is the optical power of the light source. D is a multiplied factor coming from complex IFT, with $D = 2$ in our setup.

In this configuration there are three typical noise sources: thermal noise, shot noise and beat noise. Thermal noise arises from the random thermal motion of electrons within the detector and it is usually specified by detector manufacturer. The shot noise occurs due to random distribution in arrival times (Poisson distribution) of photons at the detector. The excess intensity noise is due to the instability of the incident light associated with the random summation of different frequency components of the broadband light source. The excess intensity noise is also called the random beat frequency noise.

By extending the noise analysis of SS-OCT [18] with mismatched balanced detection [6,22] to our QSS-OCT system with the SOA inserted into on the sample arm, the mathematical expression of the photocurrent variances for each noise components is [17,21]:

$$\begin{aligned}
\left\langle \sigma^2 \right\rangle_{th} &= (NEPh)^2 \cdot B \\
\left\langle \sigma(G)^2 \right\rangle_{shot} &= e \cdot \alpha \cdot \left(P_r + P_{cs} \cdot G + P_{incs} \cdot G + P_{sp0} \cdot G\right) \cdot B \\
\left\langle \sigma(G)^2 \right\rangle_{beat} &= \frac{\alpha^2 \cdot \left[\left(P_{cs} \cdot G + P_{incs} \cdot G + P_{sp0} \cdot G\right) \cdot P_r + (1-\beta)^2 (P_r)^2\right] \cdot B}{\Delta\nu}
\end{aligned} \tag{6}$$

where, B is the detector bandwidth, $NEPh$ is the noise equivalent photocurrent density of detector, $P_r = P_0 \cdot k_1 \cdot k_2 \cdot R$ is the optical power reflected from reference arm arriving at the photodiodes, $P_{cs} = P_0 \cdot (1-k_1) \cdot k_2 \cdot S \cdot (1-X)^2$ and $P_{incs} = P_0 \cdot (1-k_1) \cdot k_2 \cdot X$ are the coherent and incoherent optical powers reflected from sample arm arriving at the photodiodes [21], P_{sp0} is the spontaneous emission power of the SOA arriving at the photodiodes when $G = 1$. β is a balanced factor and $\beta = 1$ represents a completed balanced system. If a Gaussian power spectral density source is used then $\Delta\nu$ is the effective linewidth of the source $\Delta\nu = (\pi/2\ \ln(2))^{1/2} c \cdot \Delta\lambda_{FWHM}/\lambda_0^2$ where c is the speed of light and $\Delta\lambda_{FWHM}$ is the full width at half-maximum wavelength bandwidth of the source and λ_0 is the center wavelength [5]. The first expression in Eq. (6) is thermal noise as commonly expressed. The second part is shot noise, which included all sources of power. The third expression represents the beat noise including cross-beating noise between sample and reference and the reference self-beating. The expressions in Eqs. (5) and (6) are written under the assumption of no excess losses in the system.

The SNR of our QSS-OCT system with the SOA inserted for weak sample signal amplification is described as [5,21]:

$$SNR(G) = \frac{\left\langle I(G)^2 \right\rangle}{4 \cdot \left(\left\langle \sigma^2 \right\rangle_{th} + \left\langle \sigma(G)^2 \right\rangle_{shot} + \left\langle \sigma(G)^2 \right\rangle_{beat}\right)} \tag{7}$$

where 4 accounts for the number of detectors.

4. Experimental measurements and discussion

The SNR performance of our QSS-OCT system, with the weak sample signal amplified by the SOA was evaluated by comparing the intensities of acquired A-scans with the A-scan intensities obtained without the SOA. A-scan measurements were taken using a −55 dB reflector on the sample arm. The reference mirror was adjusted to a position such that the difference in optical path length between the two interferometer arms was 500 μm. The two fiber attenuators after the 3×3 coupler were adjusted to obtain the best match of the two input optical powers for the two detectors. When the SOA was supplied with a current of 600 mA it had a gain of 30 dB. Both waveforms of interferometric signals P_1 and P_2 measured with our complex SS-OCT system with and without the SOA had sinusoidal modulations with symmetric positive and negative envelopes. Waveforms signals can be adjusted using the two attenuators in order to optimize their balance. A better Gaussian distribution was obtained from the system when using the SOA because the spectrum of SOA was closer to a Gaussian distribution than that of the swept source. The peak amplitude of the output signal when the system used the SOA was about 29 times higher than that of the system without the SOA.

Fig. 2(a) shows A-scan signals acquired with our QSS-OCT system with the SOA (solid line) and without the SOA (dashed line) in the sample arm. When the SOA was not inserted into the system, a 4 dB attenuation in the reference arm was required in order to reduce the self-beat noise from the reference light and to reach the maximum possible SNR limited by the shot noise. After the SOA, set at a 30 dB gain, was inserted in the sample arm and the attenuator was removed from the reference arm (including the appropriate optical jumper), the peak signal increased 29.7 dB from −35.2 dB to −5.5 dB, while the average noise level increased only 15.6 dB from −89.8 dB to −74.2 dB (the noise data were averaged). This results into a 14.1 dB increase in the SNR.

Fig. 2(b) shows the calculated results for various noise powers (left ordinate) and SNR (right ordinate) versus SOA gain, G, when the QSS-OCT system contains an optical amplifier. The calculations are based on the following assumptions: swept source central wavelength, FWHM bandwidth, and output power: $\lambda_0 = 1.32$ μm, $\Delta\lambda = 100$ nm, $P_0 = 20$ mW, optical power reflectance of the reference and sample arms: $R = 0$ dB, $X = S = -55$ dB, detector bandwidth: $B = 50$ MHz, noise equivalent photocurrent density: $NEPh = 2$nA/sqrt(Hz), spontaneous emission power of the SOA: $P_{sp} = P_{sp0}G$, $P_{sp0} = 10^{-3}$ mW. From the analysis shown in Fig. 2(b), when $G<15$ dB, SNR raises linearly with G because the cross-beat noise caused by reference power and the spontaneous power emission of the SOA is much smaller than the self-beat noise generated by reference power. Around $G = 18$ dB, the cross-beat noise exceeds reference self-beat noise leading to a slow SNR increase; when $G>30$ dB, the SNR saturate (see Fig. 2b). In this regime the OCT system is cross-beat noise limited. The region of interest is before the saturation where an increase in SNR ratio is predicted. The presence of the SOA has moved the OCT system from shot-noise limitation when no SOA is used to the cross-beating limitation regime. Since we are using a swept source setup, in addition to this analysis the sensitivity advantage of swept source setup must be added. Choma et al. [20] have demonstrated that for a Gaussian source an increase is expected in sensitivity compared to time domain OCT system by $M/4$ where $M = \Delta k/\delta k$ where Δk and

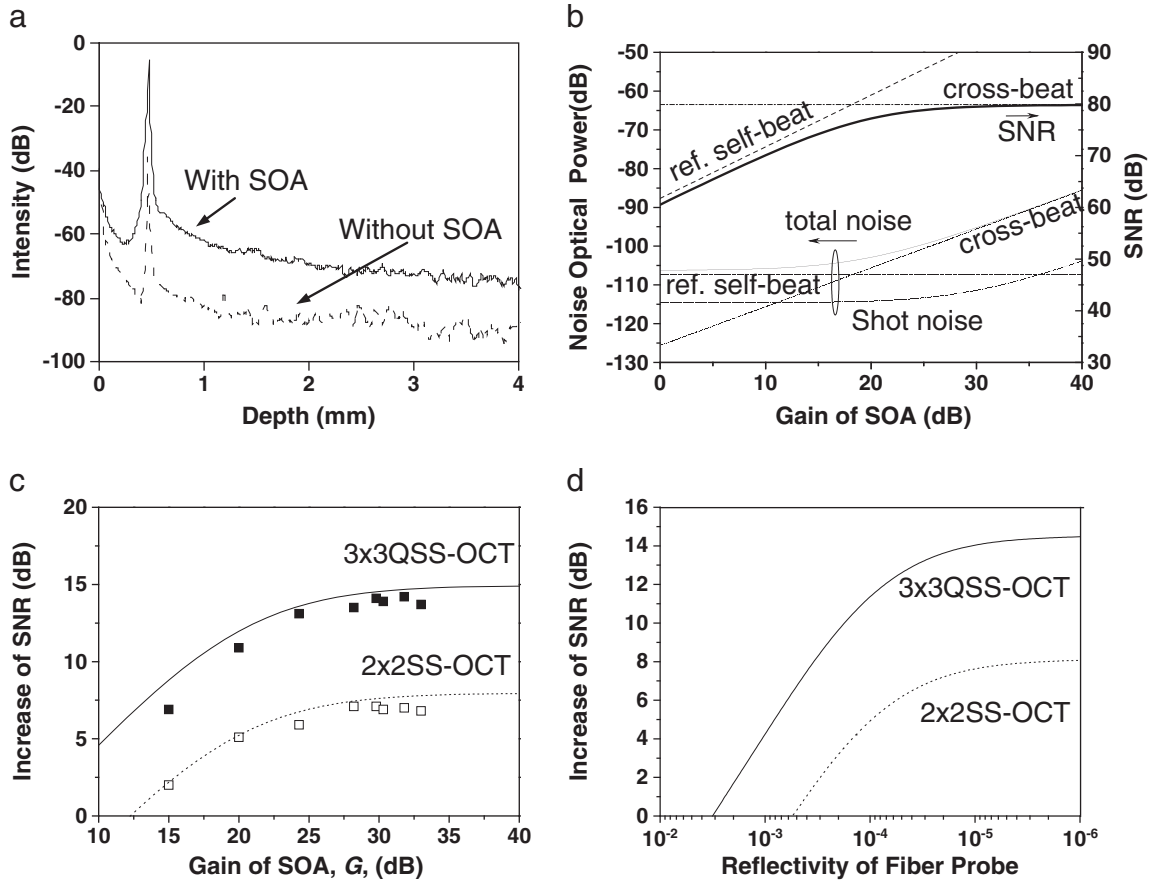

Fig. 2. (a) Measured A-scan signals from our QSS-OCT system with (solid line) and without (dashed line) an optical amplifier in the sample arm (a 10-pixel average was performed in the noise parts). (b) Theoretical results of various noise powers (left ordinate) and SNR (right ordinate) versus SOA gain, G, when the SS-OCT system contains a sample signal amplifier. (c) Calculated (solid line) and measured (solid squares) results of increase in SNR versus SOA gain, G, from our 3×3 QSS-OCT system by comparing with 2×2 OCT system. (d) Calculated increase in SNR versus the reflectivity of the fiber probe surface from our 3×3 QSS-OCT system by comparing with 2×2 OCT system.

δk are bandwidth and linewidth respectively of the light source in k-space. For our SS-OCT system this correspond to an increase of about 22 dB over the corresponding time domain OCT. The increase of SNR after the amplification can be estimated using Eq. (7) minus the commonly used shot noise limit SNR when the system without the amplifier. Calculated increase of SNR after the amplification versus SOA gain for our SS-OCT system with 3×3 quadrature interferometer and the 2×2 SS-OCT system [14,15] is shown in Fig. 2(c) together with the measured results. The experimental results agree well with the theoretical analysis. 7 dB more increase of SNR was obtained in our SS-OCT system with 3×3 quadrature interferometer than that in the 2×2 SS-OCT system. Effect of incoherent reflection from the fiber probe is investigated as well as shown in Fig. 2(d). Since SOA amplifies both coherent and incoherent, in order to get the best improvement of SNR, the reflectivity of the probe surface should be less than 10^{-5} based on our calculation. The maximum SNR increase is 15 dB and 8 dB for the 3×3 QSS-OCT and 2×2 SS-OCT systems, respectively. From Fig. 2(d) the back-reflection tolerance of both systems of 8×10^{-2} and 5×10^{-3}, respectively, was calculated.

Measurements were done at different depths by adjusting the position of reference mirror to evaluate the SNR dependence of imaging depth. SNR roll-off of 8.8 dB and 13.0 dB was obtained for systems with SOA and without SOA, respectively. After the SOA insertion into the system, the SNR increased by 14.1 dB and 18.3 dB when measured at a depth of 0.5 mm and 4 mm, respectively (Fig. 3). There is an additional 4.2 dB SNR increase at the 4 mm depth when compared to the SNR increase corresponding to the 0.5 mm depth. Therefore, the quality of images obtained from signals coming from greater depths within the sample was improved by adding an optical amplifier after sample into our QSS-OCT system.

5. Arterial plaque imaging

Watanabe heritable hyperlipidemic (WHHLMI) rabbit is a suitable animal model to study hypercholesterolemia and atherosclerosis. Arteries in these rabbits develop atheromatous plaques similar to those in humans [23]. A picture of a segment of the descending aorta together with the protected forward-view ball fiber probe [16] collecting an OCT image, is shown in Fig. 4. Fig. 5(a) shows an ex vivo OCT image of a segment of aorta where the image was acquired with the QSS-OCT system with a 25 dB gain SOA inserted in sample arm. The axial and lateral dimensions of the image are 600×900 pixels respectively which correspond to an image size of 2.5×3 mm^2. In Fig. 5(a), a clearly raised lipid core with macrophage accumulation with un-uniform reflectance within its volume (red arrows) is shown. A thin fibrous cap, which strongly scatters light, covers the lipid core (white arrow). The fibrous cap was defined as the minimum distance from the coronary artery lumen to the upper border of the lipid pool. A few calcified regions (yellow arrows) around the lipid core, characterized itself by low reflectance, are clearly discernable. The

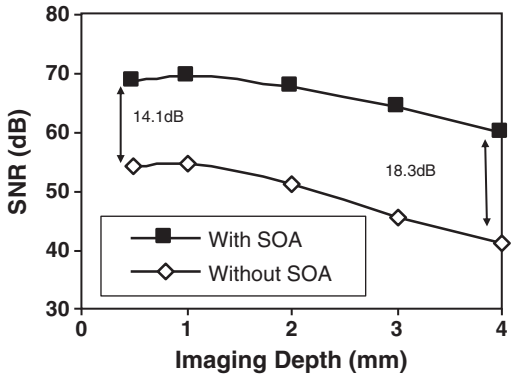

Fig. 3. Measured SNR versus imaging depth in our QSS-OCT system.

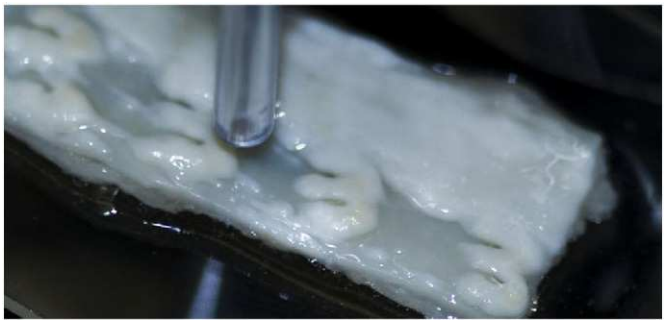

Fig. 4. An opened left descending coronary tissue from a Watanabe heritable hyperlipidemic (WHHLMI) rabbit being scanned with the forward ball lens fiber probe protected by a plastic tube.

regions with uniform reflectance (green arrows) correspond to bundles of smooth muscle cells, which can be viewed up to depths of 2 mm even beneath the calcified regions. The results obtained from images of WHHLMI coronaries acquired with our QSS-OCT, as the image shown in Fig. 5(a), agreed very well with the histological micrographs of these samples, shown in Fig. 4 of Ref. [23]. For comparison, an OCT image acquired at the same position on the sample after the SOA was extracted from the sample arm is shown in Fig. 5(b). Obviously, the image shown in Fig. 5(b) does not provide a clear view of all the clinical aspects of the sample, especially in the regions located deeper than 1 mm.

To further quantify the analysis, we selected three A-scan profiles which are illustrated in Fig. 5(c–e). These intensity profiles are shown as they were acquired with the QSS-OCT system when it had an SOA (blue) at 30 dB gain and without SOA inserted (purple). These three scans are located at the positions marked with dashed arrows in Fig. 5 (a) and (b). By comparing the data recorded when the system had the SOA with the data recorded by the system without SOA, it can be observed that the signal values increase up to 30 dB while the levels of noise increase by less than 15 dB. This increase in level of noise explains the bright appearance of the image taken with optical amplification. Signals coming from structures located at depths of up to 2 mm can be observed in the data acquired with the system that has the SOA inserted. However, structures located at and deeper than 1 mm become difficult to distinguish when the SOA is removed. The increase in the image penetration depth when acquired by the QSS-OCT with the SOA inserted is also evident in Fig. 5(a) from the ability to distinguish the lipid pool with fibrous cap, the macrophage accumulation core and the calcification boundary. The identified features can be quantified as follows: the size of macrophage accumulation core is 1.0 mm (lateral) by 0.79 mm (depth) with a 36 μm thickness the fibrous cap, while the sizes of the calcified regions are 0.6 mm by 0.4 mm (left side), 0.3 mm by 0.15 mm (right side).

6. Conclusion

We have used a semiconductor optical amplifier in the sample arm of a quadrature interferometer and balanced detection within a swept-source OCT setup. The new OCT platform produces high quality OCT images of descending aorta harvested from WHHLMI rabbits. An increase of 14 dB in signal-to-noise ratio was obtained by inserting an SOA in the sample arm of the OCT system. The penetration depth of the OCT image was increased with the addition of sample signal amplification. Preliminary results show that vulnerable plaque with fibrous caps, macrophage accumulations and calcifications present in arterial tissue are measurable with our OCT system. Our new OCT system reported in this work could help to identify the locations of vulnerable coronary plaques, in vivo, and in monitoring, with a high degree of detail, the outcomes of coronary interventions.

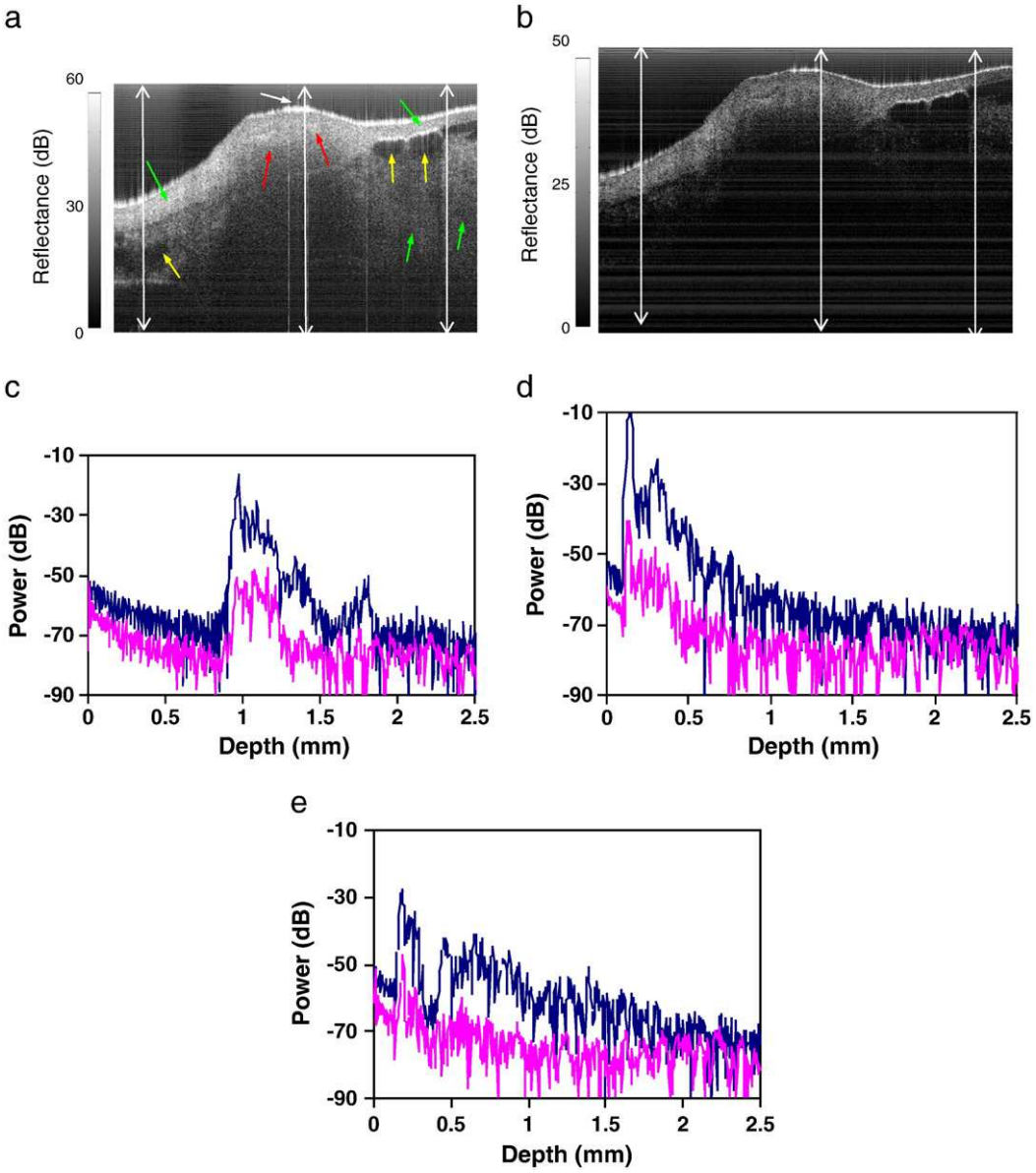

Fig. 5. Ex vivo OCT images of a coronary from a WHHLMI rabbit acquired by the QSS-OCT system with the sample signal amplifier (a) and without (b). A-scan signals at the positions of the dashed arrow lines with pixels 100 (c), 500 (d), and 680 (e) acquired by the QSS-OCT system with the sample signal amplifier (blue) and without SOA (purple).

References

[1] D. Huang, E.A. Swanson, C.P. Lin, J.S. Schuman, W.G. Stinson, W. Chang, M.R. Hee, T. Flotte, K. Gregory, C.A. Puliafito, J.G. Fujimoto, Science 254 (1991) 1178.
[2] P. Barils, J. Schmitt, Eur. Interv. 4 (2009) 529.
[3] M.V. Sarunic, M.A. Choma, C. Yang, J.A. Izatt, Opt. Express 13 (2005) 957.
[4] Y. Mao, S. Sherif, C. Flueraru, S. Chang, Appl. Opt. 47 (2008) 2004.
[5] A.M. Rollins, J.A. Izatt, Opt. Lett. 24 (1999) 1484.
[6] A.Gh. Podoleanu, Appl. Opt. 39 (2000) 173.
[7] R. Huber, M. Wojtkowski, K. Taira, J.G. Fujimoto, Opt. Express 13 (2005) 3513.
[8] J.G. Fujimoto, S.A. Boppart, G.J. Tearney, B.E. Bouma, C. Pitris, M.E. Brezinsky, Heart 82 (1999) 128.
[9] I.K. Jang, B.E. Bouma, D.H. Kang, S.J. Park, S.W. Park, K.B. Seung, K.B. Choi, M. Shishkov, K. Schlendorf, E. Pomerantsev, S.L. Houser, H.T. Aretz, G.J. Tearney, J. Am. Coll. Cardiol. 39 (2002) 604.
[10] D. Stamper, N. Weissman, M. Brezinski, J. Am. Coll. Cardiol. 47 (2006) C69.
[11] A. Luz, T. Bisceglia, C. Hughes, K. Tammam, B. Farah, J. Fajadet, Rev. Port. Cardiol. 29 (2010) 143.
[12] N.A. Patel, D.L. Stamper, M.E. Brezinski, Cardiovasc. Interventions Radiol. 28 (2005) 1.
[13] P. E. Andersen, A. Bjarklev, A. Tycho, "Optical amplification in coherent optical frequency modulated continuous wave reflectometry," US Patent, 6900943 B2 (2005).
[14] B. Rao, J. Zhang, Q. Wang, Z. Chen, Proc. SPIE 6429 (2007) 642924.
[15] P. Jayavel, T. Amano, D. Choi, H. Furukawa, H. Hiro-Oka, K. Asaka, K. Ohbayashi, Jpn. J. Appl. Phys. 45 (2006) L1317.
[16] Y. Mao, S. Chang, S. Sherif, C. Flueraru, Proc. SPIE (2008) 6826.
[17] C. Flueraru, H. Kumazaki, S. Sherif, S. Chang, Y. Mao, J. Opt. A: Pure Appl. Opt. 9 (2007) L5.
[18] R. Leitgeb, C.K. Hitzenberger, A.F. Fercher, Opt. Express 11 (2003) 889.
[19] J.F. de Boer, B. Cense, B.H. Park, M.C. Pierce, G.J. Tearney, B.E. Bouma, Opt. Lett. 28 (2003) 2067.
[20] M.A. Choma, M.V. Sarunic, C. Yang, J.A. Izatt, Opt. Express 11 (2003) 2183.
[21] H.D. Ford, R. Beddows, P. Casaubieilh, R.P. Tatam, J. Mod. Opt. 52 (2005) 1965.
[22] C.C. Rosa, A.Gh. Podoleanu, Appl. Opt. 43 (2004) 4802.
[23] M. Shiomi, T. Ito, S. Yamada, S. Kawashima, J. Fan, Arterioscler. Thromb. Vasc. Biol. 23 (2003) 1239.